*International*
*Journal*
*Of Advanced Research in Engineering& Management (IJAREM)*
*ISSN: 2456-2033 || PP. 09-19*

# Characterization of the Fe doped CDS Thin Films Produced by Ultrasonic Spray Pyrolysis Technique

S. Kurtaran[a], M. Kellegöz[b,*], S. Köse[c]

[a] *Eskisehir Osmangazi University, Faculty of Science and Letters, Department of Physics, TR-26040 Eskisehir, Turkey*

[b,*] *Eskisehir Osmangazi University, Faculty of Science and Letters, Department of Physics, TR-26040 Eskisehir, Turkey*

[c] *Eskisehir Osmangazi University, Faculty of Science and Letters, Department of Physics, TR-26040 Eskisehir, Turkey*

**Abstract:** Fe doped CdS thin films are covered on glass substrates at 340±5ºC by ultrasonic spray pyrolysis technique. Fe element incorporated into CdS precursor at volume percentages of 0 to 50% step 10. Structural, compositional, optical, surface and electrical properties of samples are analyzed using X-ray powder diffraction, scanning electron microscope, a spectroscopic ellipsometer, atomic force microscope, four-probe technique, UV/Vis and photoluminescence spectroscopy. All the samples are found to be of single-phase and crystallized in a hexagonal lattice. The x-ray diffraction peaks position of Fe doped CdS shifts to higher angle with increasing Fe concentration indicating a decrease in cell volume. It is observed the optical bandgap changes due to Fe addition. Photoluminescence technique displayed the occurrence of red emission in the CdS nanoparticles. There was a noticeable increase in the PL intensity when Fe concentration increased. Fe doped CdS samples for photovoltaic solar cells could be used as windows layer.

**Keywords:** Fe doped CdS thin film, Photovoltaic solar cells, Spray pyrolysis, Photoluminescence.

## 1. Introduction

Investigation of the structural, compositional, optical, surface and electrical properties of semiconducting samples used in electronics, optoelectronic circuit components and solar energy systems is of great importance in terms of technology. Recently, among II/VI semiconductors, cadmium sulphide (CdS) is one of the most studied compounds due to applications in, solar cells, lasers and optoelectronic devices. CdS is an important semiconductor widely used in various fields due to its optical and electrical properties. CdS samples have been extensively studied over the last few decades due to their significant optoelectronic properties [1, 2]. The direct bandgap of CdS is 2.4 eV of ambient temperature. Especially, the CdS compound has been extensively studied because of its bandgap in the visible spectral region [3]. Recently, modification of CdS properties by impurity/dopant incorporation has become a developing topic. Doping with suitable metal elements is a practical approach to adjust materials properties [4]. The doping of elements contribution of the CdS lattice has attracted the attention of many researchers. Significant results have been obtained by the doped of elements such as B [5], Ni [6], Cu [7, 8], Mn [9], Tb [10], Te [11], Gd [12], Cr [13]. Due to the additive ions, the films show a change in their structural, optical, surface and electrical properties. CdS films have been settled using many techniques such as thermal evaporation [14-16], chemical bath deposition (CBD) [17], molecular beam epitaxial (MBE) [18] and ultrasonic spray pyrolysis (USP) [19]. Among the techniques, the spray pyrolysis emerges as a very suitable one deposit semiconducting material in thin-film geometry, powders and coatings, with high quality and stability. It is of great importance to produce large surface area thin films with easy and cost-effective techniques for industrial use. In this study, we use the simple, low-cost spray pyrolysis technique to deposit the films of Fe doped CdS. Suitably analysis techniques have evaluated the effect of Fe incorporation in CdS on the structural, compositional, optical, surface and electrical properties.

## 2. Experimental details

USP method consists mainly of solution sprayed onto a heated substrate [20]. Samples were obtained by spraying on USP technique and 340±5 ºC heated glass substrate. Distilled water was used as a solvent. The

spray solution was prepared by mixing appropriate volumes of 0.1 M of cadmium chloride [$CdCl_2.H_2O$], 0.2 M of thiourea [$NH_2CSNH_2$] and 0.1 M of iron nitrate [$Fe(NO_3)_3.9H_2O$]. The 100 cc solution was sprayed onto heated microscope glass. The flow rate was fixed at 5 cc $min^{-1}$ with flowmeter. An air of 1 atm pressure was used as the carrier gas. Samples were named as CS, CSF-10, CSF-20, CSF-30, CSF-40 and CSF-50 depending on the increasing Fe addition ratio. The crystal structure of the samples was examined by a Rikagu X-ray Diffractometer (XRD), using CuKα (λ=1.5406Å) radiations. Surface morphology was analyzed by a Jeol scanning electron microscope (SEM), and the sample composition was analyzed along with energy dispersive x-ray (EDX). The optical study of the samples was carried out using a Shimadzu UV-2550 Spectrophotometer, OPT-S900 Spectroscopic Ellipsometer (SE), and the photoluminescence (PL) study, by a Perkin Elmer LS55 Fluorescence Spectrophotometer. The transmittance (T) spectra of the samples were taken at a range of 300-900 nm with UV-Vis Spectrophotometer. The diffraction indices (n), extinction coefficient (k) and thickness (t) of the samples were determined with SE. The PL was measured using Fluorescence Spectrophotometer with a Xe lamp as the excitation light source. Surface images and roughness values were studied by Park System XE-100 Atomic Force Microscopy (AFM). Keithley 2601 Lucas Labs. Pro 4 four-probe technique was used to measure the electrical resistivity of the samples.

## 3. Results and discussion

The surface images of the samples have been investigated by SEM. SEM technique in providing information about particle size and shape [20]. The microstructure of the thin film prepared by the present process was examined by SEM. The SEM micrograph of synthesized thin films is shown in Fig. 1. SEM micrographs show typical tightly adherent CdS films on glass substrates. In most cases, the final films are homogeneous, without any crack, relatively dense and exhibit almost complete coverage of the substrate. In all samples, there are distributions of different sizes and colors on the surface. It gives spherical shape, and particles distributed homogeneously. It is observed that the morphology of the samples has influenced the doping element. SEM images and EDX have been recorded using the same equipment. EDX gives information about the chemical composition of the samples. The EDX spectra of the samples and the atomic weights of Cd, S and Fe elements are given in Fig. 2. The EDX analysis reveals that Cd, Fe and S are present in the sample, and the amount of Cd decreases with increasing Fe concentration.

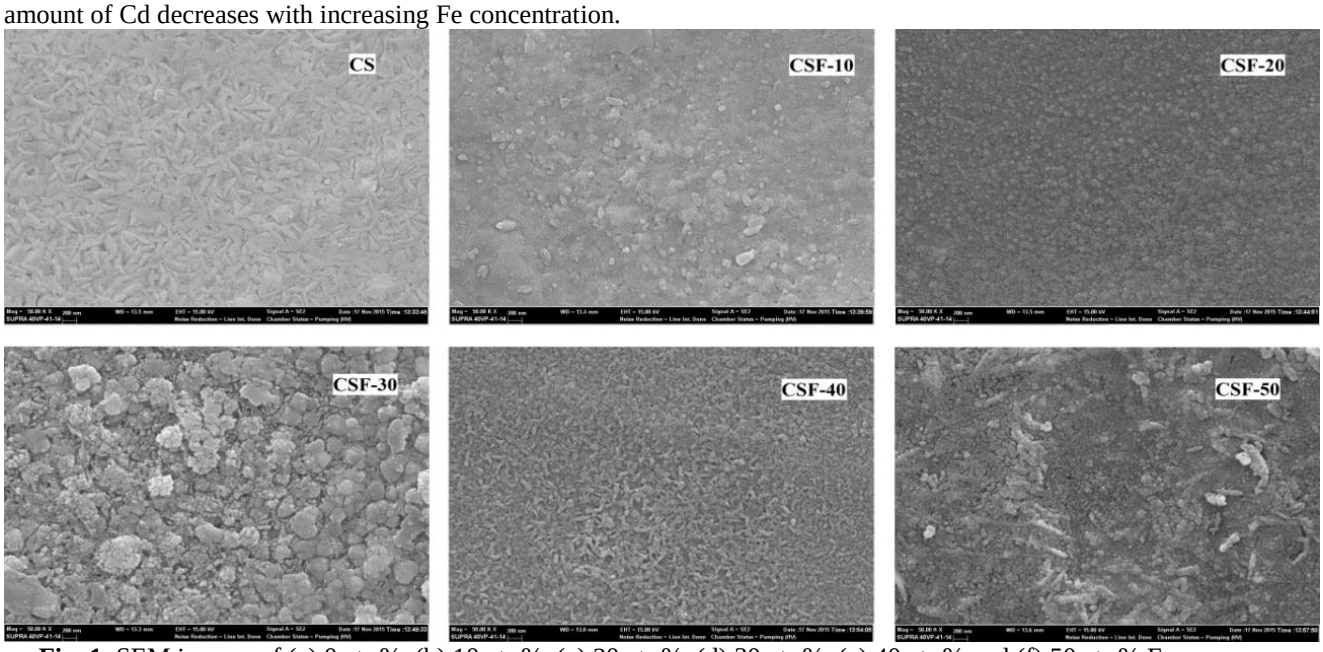


**Fig. 1.** SEM images of (a) 0 at.-%, (b) 10 at.-%, (c) 20 at.-%, (d) 30 at.-%, (e) 40 at.-% and (f) 50 at.-% Fe doped CdS thin films.

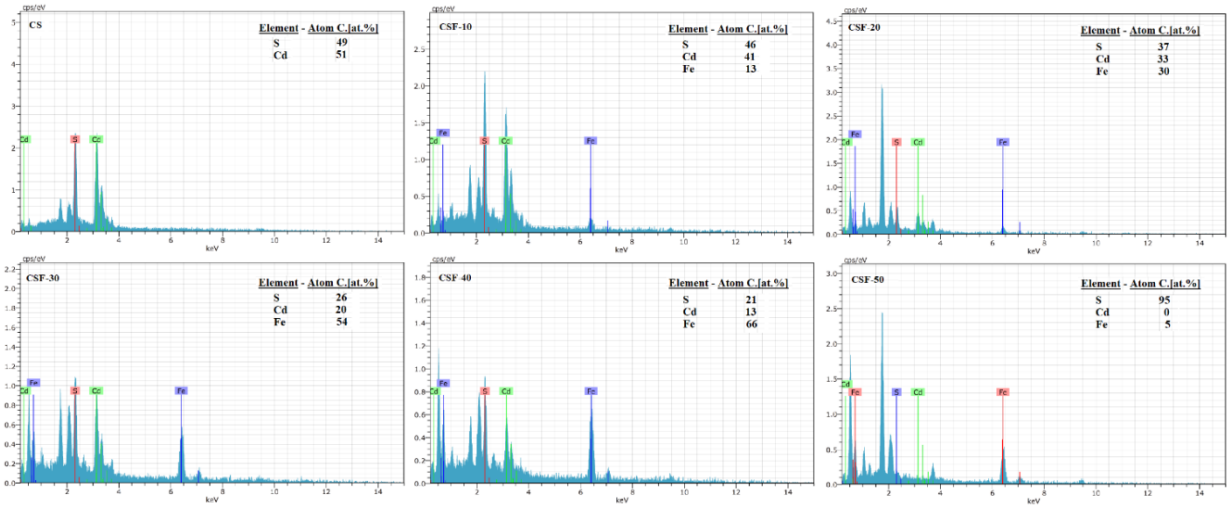


**Fig. 2.** EDX pattern of (a) 0 at.-%, (b) 10 at.-%, (c) 20 at.-%, (d) 30 at.-%, (e) 40 at.-% and (f) 50 at.-% Fe doped CdS thin films.

The XRD patterns of the samples are shown in Fig.3. The diffraction peaks are appropriately indexed as (0 1 0), (0 0 2), (0 1 1), (0 1 2), (1 1 0), (0 1 3), (1 1 2) planes. The most rugged peaks observed in XRD patterns correspond to (0 1 1) plane and additional peaks belong to (0 1 0) and (1 1 2) planes. The recorded peaks are in good agreement with the JCPDS [PDF# 98-015-4186; 98-061-9860]. As a result, the presence of these peaks suggests that the samples are in a polycrystalline and hexagonal structure. XRD patterns of the samples are broadened progressively with Fe content, indicating a decrease in crystallite size with Fe incorporation. Because the ionic radius of $Fe^{+3}$ (0.69 Å) is smaller than $Cd^{+2}$ (0.96 Å). The crystallite size ($D$) has been calculated using Scherer's formula of the samples from the powder XRD data [21].

$$D = 0.9\lambda / \beta \cos\theta \tag{1}$$

$$\langle e \rangle = (d - d_0) / d_0 \tag{2}$$

$$\delta = 1/D^2 \tag{3}$$

where 0.9 is a constant, $\beta$ is the half-peak width, $\theta$ is the Bragg's diffraction angle, $\lambda$ is the wavelength of the x-ray. The interplanar spacing, $d$, and the interplanar spacing without deformation, $d_0$, are defined in Table 1. The dislocation lines length of per unit volume of the crystal is determined by the formula (3) [22]. Small δ values mean that crystallization is good. The crystallite size ($D$), macrostrain ($< e >$)and dislocation density ($\delta$) are given in Table 2.

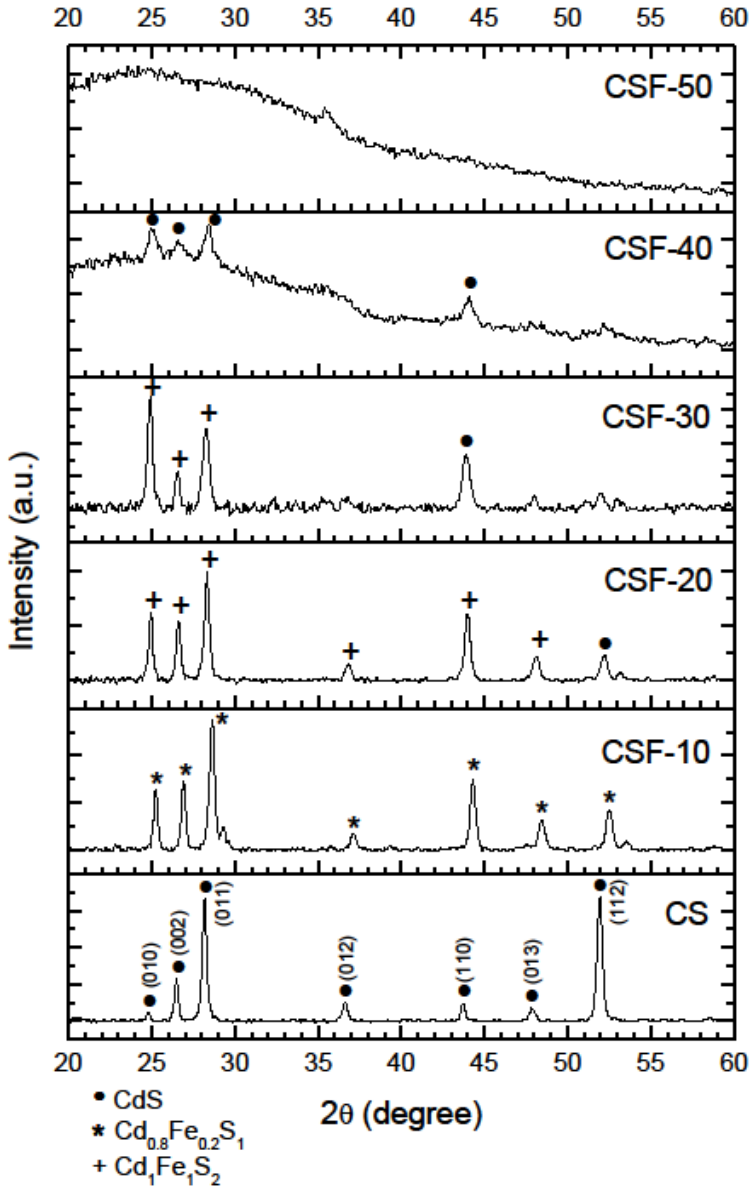


**Fig. 3.** X-ray diffraction pattern of Fe doped CdS thin films.

**Table 1.**Structural parameters of Fe doped CdS thin films.

| Sample | 2θ (°) | d (Å) | $2\theta_0$ (°) (ASTM) | $d_0$ (Å) (ASTM) | (hkl) |
|---|---|---|---|---|---|
| CS | 24.77 | 3.594 | 24.83 | 3.583 | (010) |
| | 26.49 | 3.364 | 26.52 | 3.358 | (002) |
| | 28.18 | 3.167 | 28.21 | 3.161 | (011) |
| | 36.64 | 2.453 | 36.65 | 2.450 | (012) |
| | 43.74 | 2.069 | 43.73 | 2.069 | (110) |
| | 47.88 | 1.899 | 47.88 | 1.899 | (013) |
| | 51.94 | 1.761 | 51.87 | 1.761 | (112) |
| CSF-10 | 25.24 | 3.529 | 25.19 | 3.533 | (010) |

| | | | | | |
|---|---|---|---|---|---|
| | 26.93 | 3.311 | 26.86 | 3.317 | (002) |
| | 28.64 | 3.117 | 28.61 | 3.118 | (011) |
| | 37.13 | 2.422 | 37.15 | 2.418 | (012) |
| | 44.31 | 2.044 | 44.38 | 2.039 | (110) |
| | 48.44 | 1.879 | 48.53 | 1.874 | (013) |
| | 52.53 | 1.742 | 51.71 | 1.766 | (112) |
| CSF-20 | 24.94 | 3.570 | 25.19 | 3.533 | (010) |
| | 26.62 | 3.349 | 26.86 | 3.317 | (002) |
| | 28.33 | 3.149 | 28.61 | 3.118 | (011) |
| | 36.86 | 2.439 | 37.15 | 2.418 | (012) |
| | 43.99 | 2.058 | 44.38 | 2.039 | (110) |
| | 48.12 | 1.891 | 48.53 | 1.874 | (013) |
| | 52.22 | 1.752 | 51.71 | 1.766 | (112) |
| CSF-30 | 24.91 | 3.575 | 25.19 | 3.533 | (010) |
| | 26.54 | 3.359 | 26.86 | 3.317 | (002) |
| | 28.29 | 3.154 | 28.61 | 3.118 | (011) |
| | 43.89 | 2.062 | 44.38 | 2.039 | (110) |
| CSF-40 | 25.07 | 3.552 | 25.19 | 3.533 | (010) |
| | 26.63 | 3.348 | 26.86 | 3.317 | (002) |
| | 28.43 | 3.139 | 28.61 | 3.118 | (011) |
| | 44.04 | 2.056 | 44.38 | 2.039 | (110) |

**Table 2.** Crystallite size (D), dislocation density ($\delta$) and macrostrain <*e*> of Fe doped CdS thin films.

| **Sample** | **(hkl)** | ***D* (Å)** | **$\delta$x10$^{-5}$(Å$^{-2}$)** | **<*e*>** |
|---|---|---|---|---|
| CS | (011) | 303 | 1.089 | 0.0019 |
| | (112) | 325 | 0.947 | 0.0012 |
| CSF-10 | (011) | 302 | 1.096 | -0.0032 |
| CSF-20 | (011) | 226 | 1.958 | 0.0099 |
| CSF-30 | (010) | 295 | 1.149 | 0.0119 |
| | (011) | 249 | 1.613 | 0.0116 |
| CSF-40 | (011) | 227 | 1.941 | 0.0067 |

**Table 3.**Cauchy-Urbach model parameters, thickness values and average values of optical constants of Fe doped CdS thin films.

| **Sample** | ***t* (nm)** | **$A_n$** | **$B_n$ (nm)$^2$** | **$C_n$ (nm)$^4$** | **$A_k$** | **$B_k$ (eV)$^{-1}$** | **n** | **k** |
|---|---|---|---|---|---|---|---|---|
| CS | 48 | 2.105 | 0.015 | 0.001 | 0.104 | 1.501 | 2.113 | 0.009 |
| CSF-10 | 65 | 2.361 | 0.235 | 0.389 | 0.104 | 1.501 | 2.593 | 0.009 |
| CSF-20 | 80 | 2.212 | 0.404 | -0.091 | 0.104 | 1.501 | 2.397 | 0.009 |
| CSF-30 | 193 | 2.629 | 0.401 | -0.015 | 0.156 | 1.509 | 2.834 | 0.016 |
| CSF-40 | 317 | 1.924 | 0.033 | -0.201 | 0.156 | 1.509 | 1.884 | 0.016 |
| CSF-50 | 301 | 2.356 | 0.035 | -0.053 | 0.156 | 1.509 | 2.359 | 0.016 |

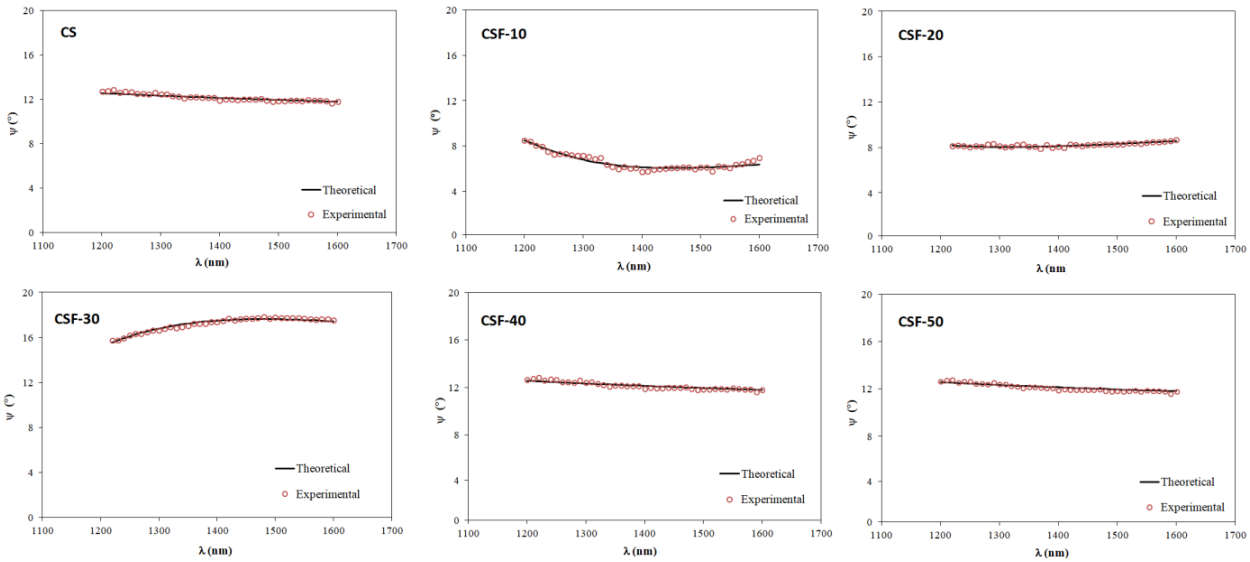


**Fig. 4.** Spectroscopic ellipsometry (SE) spectra of Fe doped CdS thin films.

One of the analyses used to identify thin films is the mighty non-destructive SE [20]. Ellipsometric measurements are collected at an angle of incidence of 50°-70° across the spectral range 1200-1600 nm. $\psi$parameter is measured as a function of the wavelength. For samples affected by depolarization, the angle of arrival is an essential factor. The best angle was determined as 70°, by using the experimental $\psi$spectra. The Cauchy-Urbach distribution model is used for adaptation to the experimental data [8].Then, the parameters ($A_n$, $B_n$, $C_n$, $A_k$, $B_k$) of the Cauchy-Urbach model are given in Table 3. When $\psi$ spectrums are reviewed, it may be said that the coherence between the theoretical model and experimental data is good. But in the samples, it draws attraction that there are deviations at experimental and theoretical $\psi$ values which is given are Fig. 4. Such a variation may have been occurred due to that the data taken in the spectroscopic ellipsometer technique is sensitive to surfaces of the films.

The transmittance spectra of the samples have been investigated at a wavelength of 300-900 nm at room temperature. Transmittance spectra are shown in Fig. 5. The band gaps of the samples have been found by the optical method[23, 24]. In Fig. 6, $(\alpha h\upsilon)^2 \sim h\upsilon$ variations have been plotted where band gap values have been computed by extrapolating the linear portions to $(\alpha h\upsilon)^2=0$. Table 4 shows the bandgap values of the samples. But there is no regular trend in the band gap with increasing of dopant concentration. The decrease in the bandgap depends on the new energy levels caused by doping.

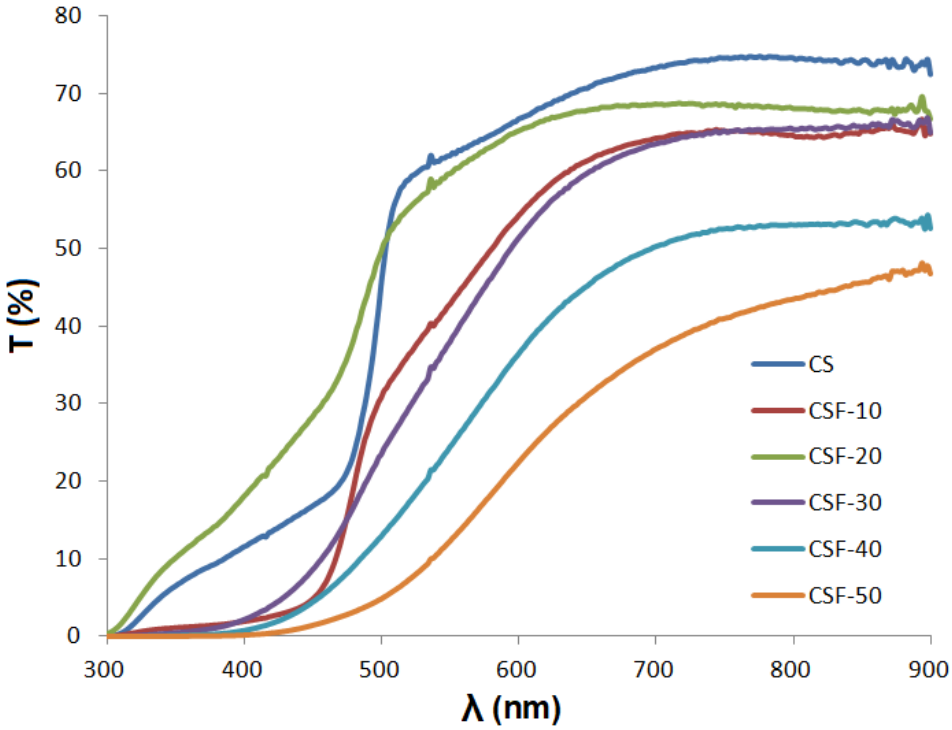


**Fig. 5.** Optical transmittance spectra of Fe doped CdS thin films.

**Table 4.** Optical band gap values of Fe doped CdS thin films.

| Sample | $E_g$(eV) |
|---|---|
| CS | 2.45 |
| CSF-10 | 2.47 |
| CSF-20 | 2.39 |
| CSF-30 | 2.32 |
| CSF-40 | 2.10 |
| CSF-50 | 2.28 |

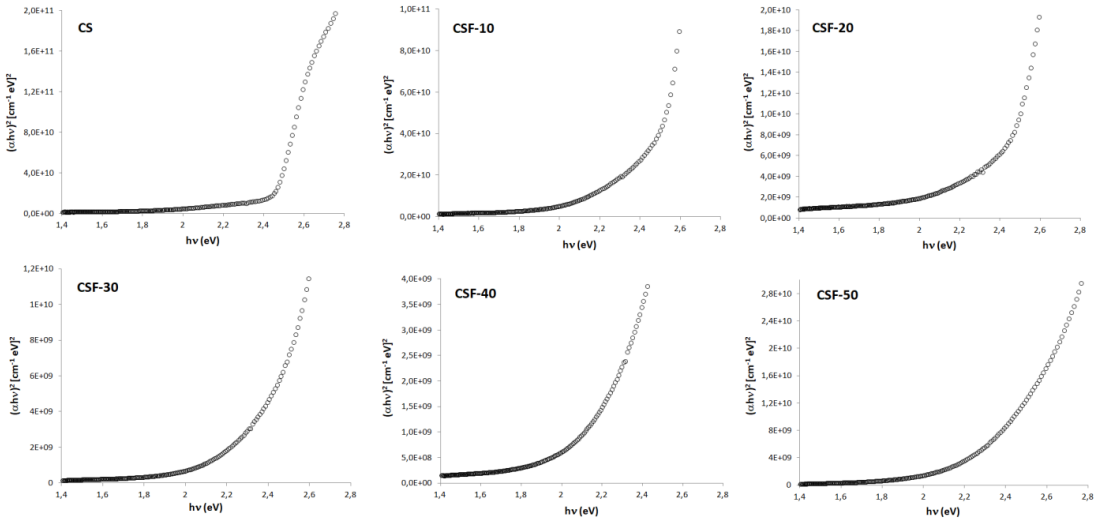


**Fig.6.** ($\alpha h\upsilon^2$ vs $h\upsilon$ alteration graphics of Fe doped CdS thin films.

PL spectroscopy is a sensitive technique to explore structural defects. Bandgap, phase change and density of defects are determined by PL [25]. Fig. 7 shows the PL spectra of the samples taken at room temperature for the excitation wavelength of 400 nm. The PL spectra of the samples showed emission peaks at about 480, 530 and 600 nm, respectively. A weaker blue emission band located at ~475nm and weaker green emission band at ~525 nm were observed. The blue emission band is attributed to the radioactive transition of defect states such as sulphur vacancies [26]. The green emission band can be related to impurity ions[27, 28]. Fe doping occupies the Cd lattices site

Fig. 7 shows a broad peak centered at about 600 nm that includes orange bands. The peak observed at 600 nm corresponds to radiation recombination with shallow levels in the bandgap due to natural impurities [29]. As shown in PL spectra of the samples, the PL intensity enhanced with increasing $Fe^{+3}$ concentrations. In the samples, more electron-hole pairs are formed. Due to the recombination of the electron-hole pairs and more photon emission, the fluorescence intensity is increased.

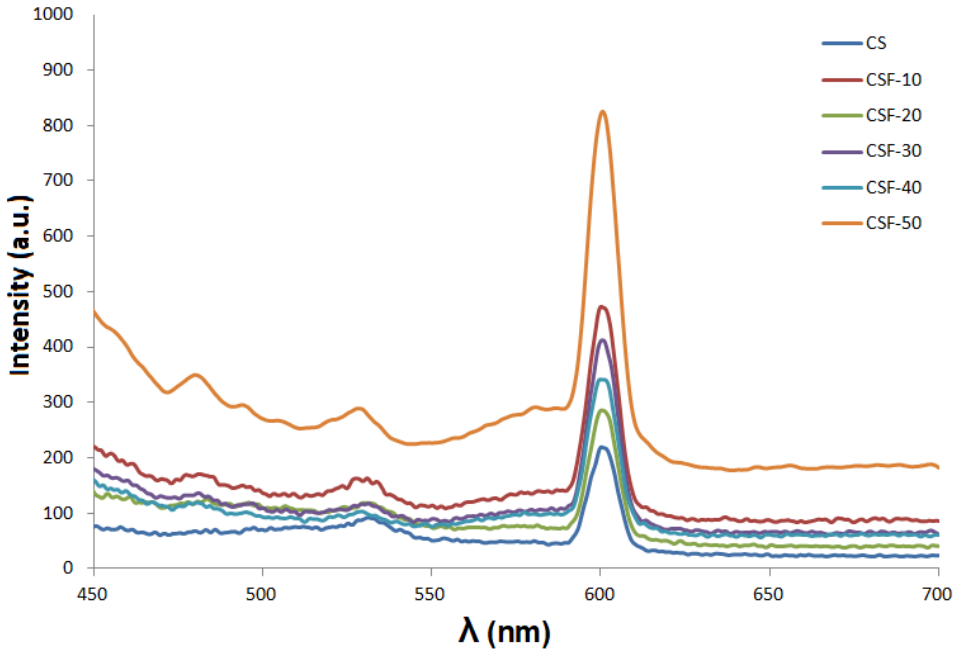


**Fig.7.** PL spectra of Fe doped CdS thin films.

Fig. 8 shows AFM images of the samples. AFM images of 5x5 $\mu m^2$ are presented of the samples. It is that the dominant growth mechanism is island-like formation for all samples. There are clusters in different height and size through the surfaces of the samples. Black regions in these images represent the crack and voids, where the sample continuity suffers. The roughness of AFM images is visible. Roughness values $R_q$(root mean square, RMS) and $R_a$(average) of the samples are given in Table 5. Sample CSF-40 has the lowest roughness value, among others. This is a desired property for solar cell applications, which will reduce the short circuit effects.

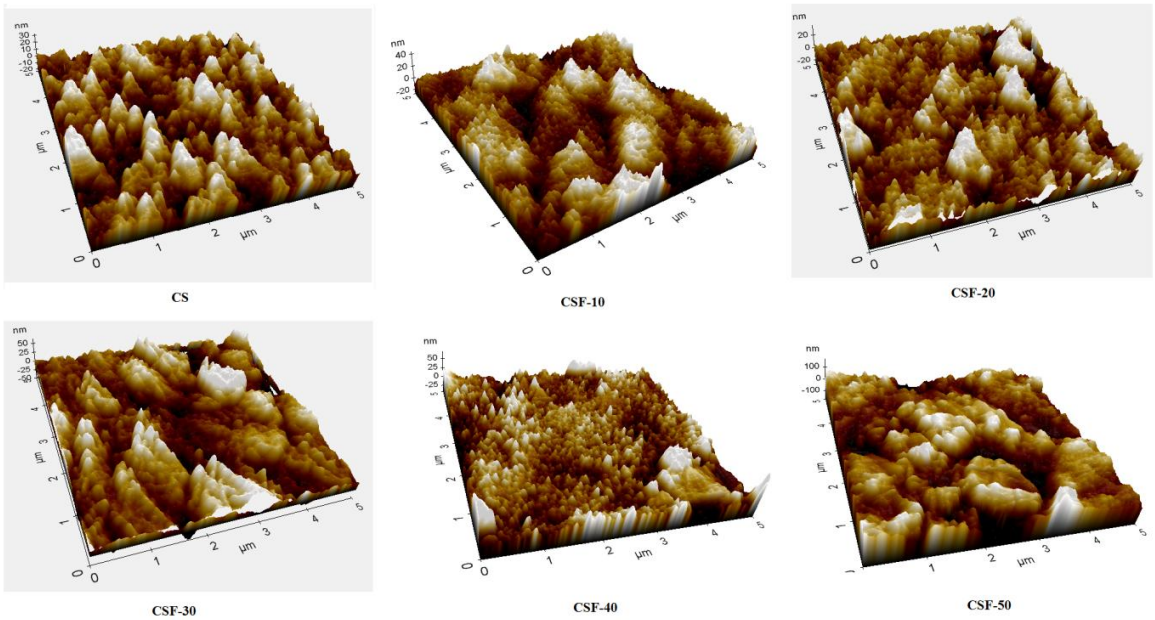


**Fig. 8.** AFM images of Fe doped CdS thin films.

**Table 5.** Roughness values of Fe doped CdS thin films.

| Sample | $R_a$(nm) | $R_q$(nm) |
|---|---|---|
| CS | 6 | 8 |
| CSF-10 | 8 | 10 |
| CSF-20 | 7 | 9 |
| CSF-30 | 13 | 16 |
| CSF-40 | 7 | 10 |
| CSF-50 | 29 | 37 |

The four-probe techniques are used to find the resistivity of the samples. As shown in Table 6, the resistivity of the samples increased with increasing Fe doping concentration. The sample CSF-40 maximum resistivity while CS has the lowest resistivity at room temperature among all the samples. It is found that on increasing the $Fe^{+3}$ concentrations in CdS nanoparticles, current increases, which may be due to incorporating the iron impurity for Cd cites and availability of free electrons.

**Table 6.** Resistivity values of Fe doped CdS thin films.

| Sample | □ (□cm) |
|---|---|
| CS | $8.26x10^4$ |
| CSF-10 | $1.22x10^5$ |
| CSF-20 | $1.49x10^5$ |
| CSF-30 | $1.43x10^5$ |
| CSF-40 | $2.24x10^5$ |
| CSF-50 | $1.81x10^5$ |

## 4. Conclusion

CdS and CdS:Fe thin films have been deposited successfully onto glass substrates using USP technique. The effects of the Fe concentration on the structural, optical, surface and electrical, properties of the samples are investigated. XRD studies are showing a single phase with a hexagonal structure. Fe doping has a significant effect on the crystalline quality and grain size of samples. Grain size decreases as Fe concentration increases. EDX pattern shows that doping has been properly doped to the CdS lattice. All samples have been determined to have a direct bandgap structure. Surface morphology has shown that samples are a smooth

surface. PL spectra show that emission intensity is increased $Fe^{+3}$ doping concentration increases. It has seen that the thickness value of the samples increased, and there is a decrease in transmittance values. Fe incorporation caused the samples of the films to have high resistivity. This is an improvement as CdS known to be a high resistivity material, which causes lower efficiency when used as a window layer. Fe incorporation at a high rate (sample CSF-50), caused distorted surfaces with voids. However, sample CSF-20 has a uniform surface with low roughness values. Production of Fe doped CdS thin films and determination of their parameters are still in progress.

## References

[1]. M. Thambidurai, N. Muthukumarasamy, S. Agilan, N. Murugan, N.S. Arul, S. Vasantha, R. Balasundaraprabhu, Studies on optical absorption and structural properties of Fe doped CdS quantum dots, Solid State Sci 12(9) (2010) 1554-1559.

[2]. A.A. Yadav, M.A. Barote, E.U. Masumdar, Studies on nanocrystalline cadmium sulphide (CdS) thin films deposited by spray pyrolysis, Solid State Sci 12(7) (2010) 1173-1177.

[3]. S.J. Ikhmayies, R.N. Ahmad-Bitar, Dependence of the photoluminescence of CdS:In thin films on the excitation power of the laser, J Lumin 149 (2014) 240-244.

[4]. S.M.T. Otoqsara, M.H. Yusefi, A.A. Khosravi, Optical characterization of Fe3+ doped CdS nanoparticles synthesized by wet-chemical route, Turkish Journal of Physics 35 (2011) 341.

[5]. M. Kellegoz, H. Çako, S. Uzkalan, S. Kose, Investigation of Boron-Doped CdS Films Deposited by Ultrasonic Spray Pyrolysis Technique, Afyon Kocatepe University-Science and Engineering 18 (2018) 441.

[6]. F. Atay, S. Kose, V. Bilgin, I. Akyuz, CdS : Ni films obtained by ultrasonic spray pyrolysis: effect of the Ni concentration, Mater Lett 57(22-23) (2003) 3461-3472.

[7]. K.S. Rathore, D.D. Patidar, N.S. Saxena, K.B. Sharma, EFFECT OF Cu DOPING ON THE STRUCTURAL, OPTICAL AND ELECTRICAL PROPERTIES OF CdS NANOPARTICLES, J Ovonic Res 5(6) (2009) 175-185.

[8]. S. Kose, F. Atay, V. Bilgin, I. Akyuz, E. Ketenci, Optical characterization and determination of carrier density of ultrasonically sprayed CdS:Cu films, Appl Surf Sci 256(13) (2010) 4299-4303.

[9]. Z. Jindal, N.K. Verma, Effect of Mn Doping on Solvothermal Synthesis of CdS Nanowires, Materials Sciences and Applications 1 (2010) 210.

[10]. S. Rai, L. Bokatial, Effect of CdS nanoparticles on photoluminescence spectra of Tb3+ in sol-gel-derived silica glasses, B Mater Sci 34(2) (2011) 227-231.

[11]. W.Z. Wu, H.A. Ye, X.L. Ruan, Luminescence dynamics of Te doped CdS quantum dots at different doping levels, Nanotechnology 21(26) (2010).

[12]. M. Thambidurai, N. Muthukumarasamy, D. Velauthapillai, C. Lee, Quantum confinement effects in Gd-doped CdS nanoparticles prepared by chemical precipitation technique, J Mater Sci-Mater El 24(11) (2013) 4535-4541.

[13]. K.S. Kumar, A. Divya, P.S. Reddy, Synthesis and characterization of Cr doped CdS nanoparticles stabilized with polyvinylpyrrolidone, Appl Surf Sci 257(22) (2011) 9515-9518.

[14]. G.B. Smith, A. Ignatiev, G. Zajac, Solar Selective Black Cobalt - Preparation, Structure, and Thermal-Stability, J Appl Phys 51(8) (1980) 4186-4196.

[15]. A.O. Caldeira, A.J. Leggett, Influence of Dissipation on Quantum Tunneling in Macroscopic Systems, Phys Rev Lett 46(4) (1981) 211-214.

[16]. K. Chidambaram, L.K. Malhotra, K.L. Chopra, Spray-Pyrolyzed Cobalt Black as a High-Temperature Selective Absorber, Thin Solid Films 87(4) (1982) 365-371.

[17]. C. Nethravathi, S. Sen, N. Ravishankar, M. Rajamathi, C. Pietzonka, B. Harbrecht, Ferrimagnetic Nanogranular Co3O4 through Solvothermal Decomposition of Colloidally Dispersed Monolayers of α-Cobalt Hydroxide, The Journal of Physical chemistry. B 109(23) (2005) 11468.

[18]. J. Nishino, T. Kawarada, S. Ohshio, H. Saitoh, K. Maruyama, K. Kamata, Conductive indium-doped zinc oxide films prepared by atmospheric-pressure chemical vapour deposition, J Mater Sci Lett 16(8) (1997) 629-631.

[19]. W.S. Hu, Z.G. Liu, X.L. Guo, C. Lin, S.N. Zhu, D. Feng, Preparation of c-axis oriented ZnO optical waveguiding films on fused silica by pulsed laser reactive ablation, Material Letters 25 (1995) 5.

[20]. F. Atay, V. Bilgin, I. Akyuz, S. Kose, The effect of In doping on some physical properties of CdS films, Mat Sci Semicon Proc 6(4) (2003) 197-203.
[21]. S.D. Gunjal, Y.B. Khollam, S.A. Arote, S.R. Jadkar, P.N. Shelke, K.C. Mohite, Structural, Optical and Electrical Properties of Spray Pyrolysis Deposited CdS Films, Macromolecular Symposia 347 (2015) 9.
[22]. A.A. Dakhel, Transparent conducting properties of samarium-doped CdO, J Alloy Compd 475(1-2) (2009) 51-54.
[23]. G.S. Lotey, N.K. Verma, Fabrication and characterization of Cu-CdSe-Cu nanowire heterojunctions, J Nanopart Res 13(10) (2011) 5397-5405.
[24]. K. Kaur, G.S. Lotey, N.K. Verma, Optical and magnetic properties of Fe-doped CdS dilute magnetic semiconducting nanorods, J Mater Sci-Mater El 25(6) (2014) 2605-2610.
[25]. J. Hasanzadeh, S.F. Shayesteh, Luminescence of doped CdS nanocrystals: effect of doping and capping agent, Opt Appl 41(4) (2011) 921-928.
[26]. M.G.S.B. Ahamed, A.R. Balu, V.S. Nagarethinam, A. Thayumanavan, K.R. Murali, C. Sanjeeviraja, M. Jayachandran, Structural, optical, and electrical properties of electron beam evaporated CdSe thin films, Cryst Res Technol 45(4) (2010) 387-392.
[27]. W.P. Bleha, R.M. Peacock, Photoluminescent Properties of Vacuum- Deposited Cadmium Sulfide Films, J Appl Phys 41 (1970) 4992.
[28]. O. Vigil, I. Riech, M. GarciaRocha, O. ZelayaAngel, Characterization of defect levels in chemically deposited CdS films in the cubic-to-hexagonal phase transition, Journal of Vacuum Science & Technology a-Vacuum Surfaces and Films 15(4) (1997) 2282-2286.
[29]. C.N.P. Dafonseca, M.A. Depaoli, A. Gorenstein, Electrochromism in Cobalt Oxide Thin-Films Grown by Anodic Electroprecipitation, Sol Energ Mat Sol C 33(1) (1994) 73-81.